

Supplemental information

**NudC guides client transfer between the Hsp40/70
and Hsp90 chaperone systems**

Maximilian M. Biebl, Florent Delhommel, Ofrah Faust, Krzysztof M. Zak, Ganesh Agam, Xiaoyan Guo, Moritz Mühlhofer, Vinay Dahiya, Daniela Hillebrand, Grzegorz M. Popowicz, Martin Kampmann, Don C. Lamb, Rina Rosenzweig, Michael Sattler, and Johannes Buchner

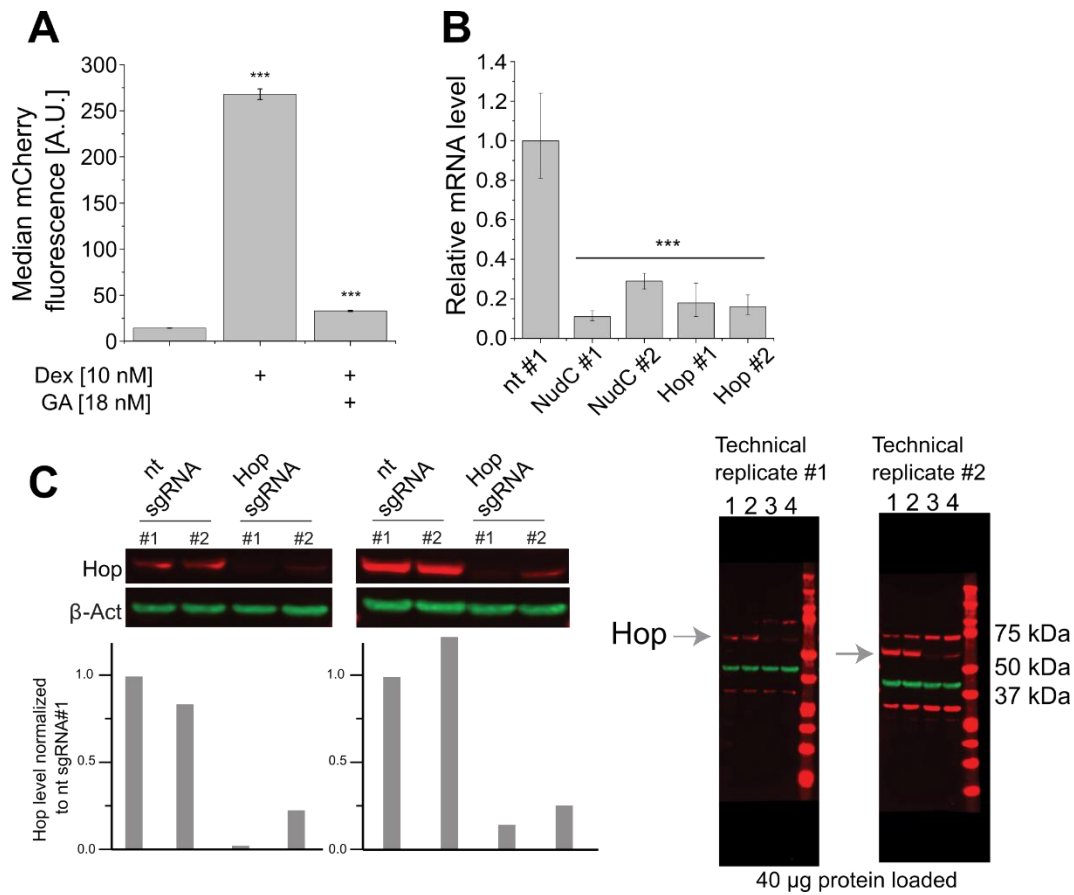


Figure S1: Chemical inhibition of Hsp90 and knockdown of co-chaperones (Related to Figure 1)

(A) Hsp90 inhibition suppresses GR activation. The activation of GR in K562 cells expressing mCherry as a reporter for GR activity was measured after 24 h treatment with dexamethasone (Dex) and geldanamycin (GA) as shown. GR activity was quantified by the median mCherry fluorescence determined by flow cytometry. Shown are the means and SD of three biological triplicates. Statistical significance was determined by student-t-test (n.s. $p \geq 0.05$; * $p < 0.05$, ** $p < 0.01$, *** $p < 0.001$).

(B) Quantification of knockdown efficiencies. K562 cells were transduced with the indicated sgRNAs using lentiviral infection. The mRNA levels after knockdown were analyzed by qPCR and normalized to the nt #1 control sgRNA in K562 cells overexpressing GR. Shown are the means and SD of three biological triplicates. Statistical significance was determined by student-t-test (n.s. $p \geq 0.05$; * $p < 0.05$, ** $p < 0.01$, *** $p < 0.001$). (nt = non-targeting)

(C) Quantification of Hop knockdown. The levels of Hop after sgRNA-mediated knockdown were analyzed by Western-Blot (red). Beta-Actin was quantified as a loading control (green).

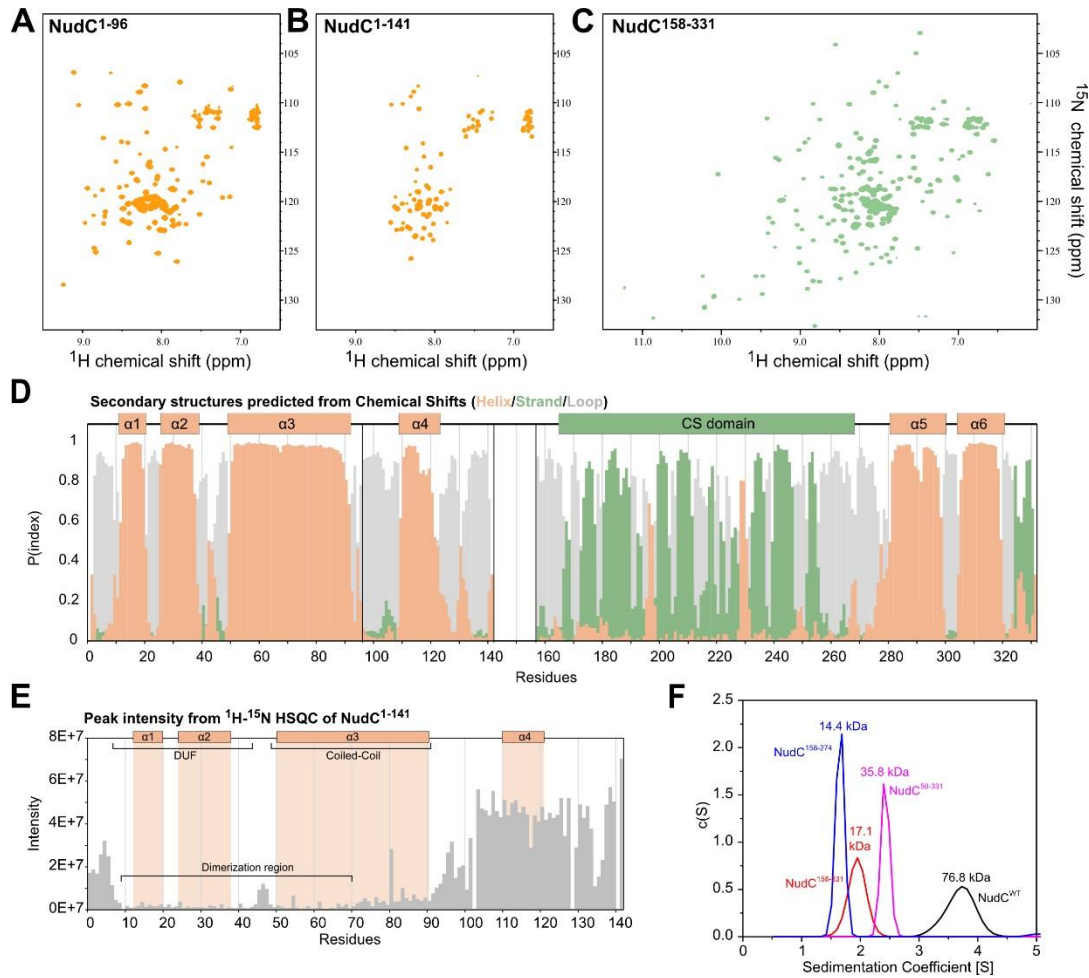


Figure S2: Domain Architecture of NudC (Related to Figure 2)

(A) ^1H - ^{15}N HSQC spectrum of NudC¹⁻⁹⁶.

(B) ^1H - ^{15}N HSQC spectrum of NudC¹⁻¹⁴¹ shown at low contour level so that only the most intense peaks, corresponding to flexible regions, are visible.

(C) ^1H - ^{15}N HSQC spectrum of NudC¹⁵⁸⁻³³¹ (comprising the CS domain and the C-terminal region).

(D) Secondary structure propensity of NudC sequence determined from backbone secondary chemical shifts ($^1\text{H}^{\text{N}}$, ^{15}N , $^{13}\text{C}\alpha$, $^{13}\text{C}\beta$, ^{13}CO) for the constructs shown in (A). For the N-terminal region the secondary structure for residues 1-96 was determined from NudC¹⁻⁹⁶ and for residues 97-141 based on the NudC¹⁻¹⁴¹ construct. The prediction shows four helices in the N-terminal half of NudC, $\alpha1$ and $\alpha2$ are part of the DUF, the coiled-coil corresponds to helix $\alpha3$ and the last helix $\alpha4$ is newly identified here, but was previously thought to be part of the coiled-coil.

(E) Relative signal intensities for backbone amides in the ^1H - ^{15}N HSQC spectrum of NudC¹⁻¹⁴¹. The lowest peak intensities are observed in the region 10-70, including helices $\alpha1$, $\alpha2$ and $\alpha3$. Beyond this, signal intensities gradually increase in the $\alpha3$ - $\alpha4$ linker and are high until the C-terminal region of this construct, indicating that the helix $\alpha4$ is flexible and independent from the first three helices.

(F) Analytical ultracentrifugation analysis of various NudC fragments to determine the dimerization region. The sedimentation coefficient of different NudC fragments was analyzed by absorption aUC. Only the construct including the first 50 residues is able to dimerize in solution, indicating that the coiled-coil region is not sufficient to trigger the dimerization and that the helices $\alpha1$ and $\alpha2$ from the DUF are also required. [NudC^{WT}: 15.7 μM , NudC¹⁵⁸⁻³³¹: 15.7 μM , NudC¹⁵⁸⁻²⁷⁴: 16.7 μM , NudC⁵⁰⁻³³¹: 15.7 μM].

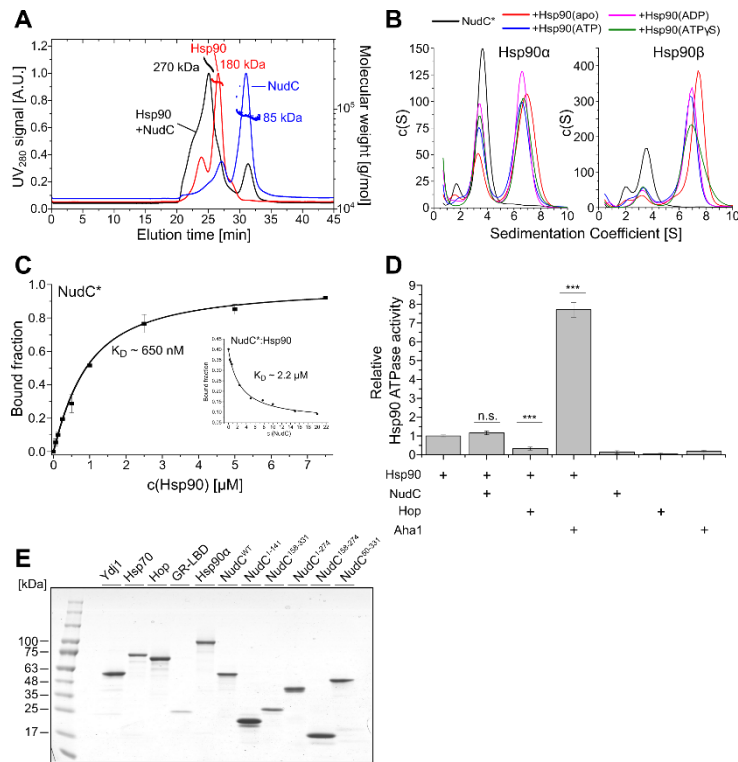


Figure S3: NudC interacts with Hsp40 and Hsp90 (Related to Figure2)

(A) Dimeric NudC binds to the Hsp90 dimer. The SEC-MALS chromatograph of Hsp90, NudC and a sample containing both NudC and Hsp90 is shown. The estimated masses are indicated. The samples were mildly crosslinked with 0.025% glutardialdehyde for 5 minutes before measurement. Note that high-order oligomers of NudC and Hsp90 eluting as minor peaks or a shoulder are a consequence of the crosslinking reaction. [NudC: 35 μ M, Hsp90 α : 35 μ M].

(B) NudC interacts with Hsp90 α in all nucleotide states. The binding of Hsp90 α with labelled NudC was analyzed by aUC in the presence of the indicated nucleotides at a concentration of 2 mM. A small peak at ~1 S is visible in some samples and represents a labeled NudC monomer. [NudC*: 500 nM, Hsp90 α / β : 5 μ M].

(C) NudC binds Hsp90 with high affinity. Triplicates of Hsp90 α titrated to labelled NudC* (500 nM) were analyzed by aUC in the absence of nucleotides. Data was fitted with a quadratic fit function to determine the dissociation constant. Data represent means \pm SD from three independent measurements. Inset: A competition titration in which unlabeled NudC was titrated to a complex between NudC* (500 nM) and Hsp90 α (900 nM dimer) was analyzed by aUC yielding a similar dissociation constant, suggesting that the fluorescent label only has little effect on the interaction between NudC and Hsp90.

(D) NudC does not affect Hsp90 ATPase. The effects of NudC, Aha1 and Hop on the ATPase of human Hsp90 α were analyzed with a regenerative ATPase assay. All components were used at a concentration of 10 μ M and the background ATPase after Hsp90 inhibition was subtracted. Control measurements without Hsp90 are shown. Statistical significance was determined by student-t-test (n.s. $p \geq 0.05$; * $p < 0.05$, ** $p < 0.01$, *** $p < 0.001$).

(E) Coomassie staining of purified protein preparations. The indicated proteins were purified and analyzed by SDS-PAGE and Coomassie staining to estimate the protein purity. Approximately 1-2 μ g of protein were loaded.

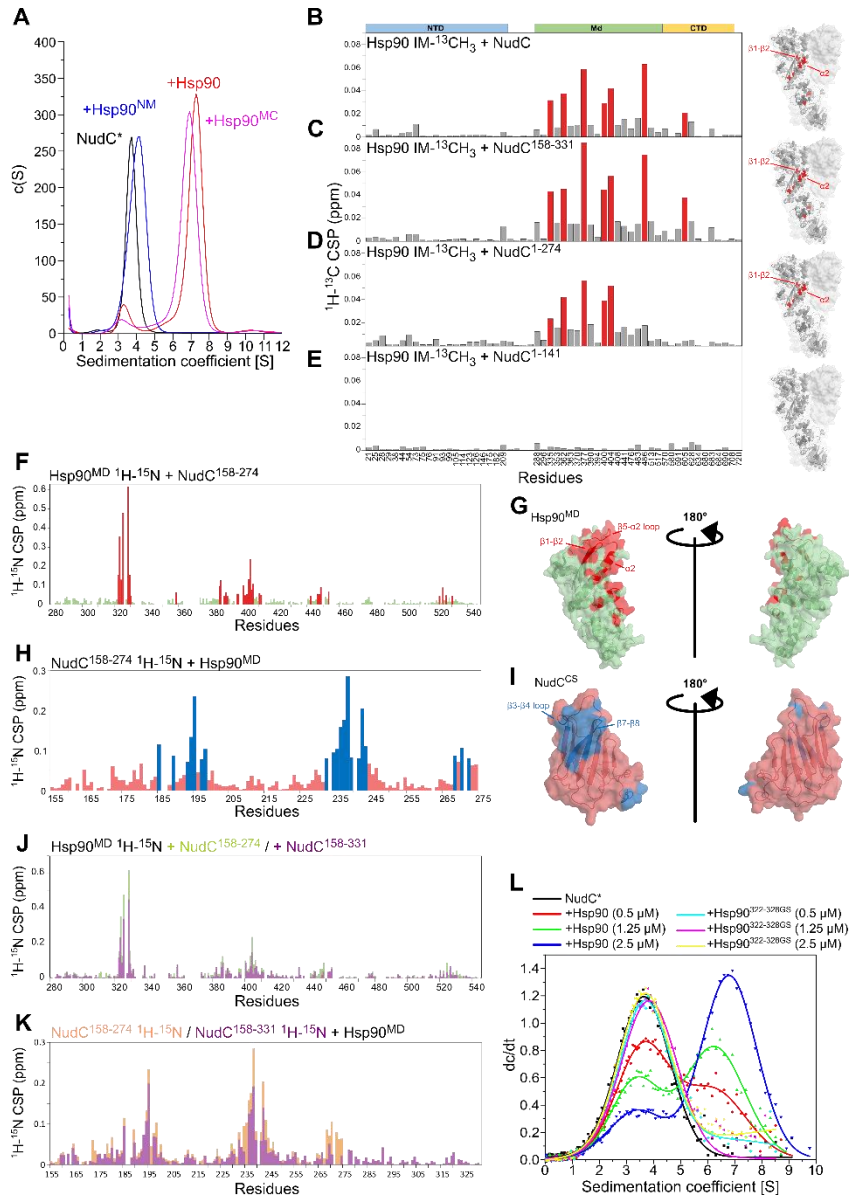


Figure S4: Interaction of NudC fragments with Hsp90 IM $^{13}\text{CH}_3$ (Related to Figure 2)

(A) Binding of NudC to Hsp90 fragments. The binding of Atto488-labeled NudC* to the Hsp90 β^{NM} and Hsp90 β^{MC} fragments was analyzed by aUC in the absence of nucleotide. [NudC*: 500 nM, Hsp90 β and mutants: 4 μM]

(B) Chemical shift perturbations of Hsp90 $^{13}\text{CH}_3$ -IM resonances upon addition of unlabeled NudC. Bar graphs showing CSPs of Hsp90 labeled residues along the sequence. Residues without CSP or change of intensity are shown in grey, residues with significant CSP are shown in red.

(C) Chemical shift perturbations of Hsp90 $^{13}\text{CH}_3$ -IM resonances upon addition of unlabeled NudC $^{158-331}$. Bar graphs showing CSPs of Hsp90 labeled residues along the sequence. Residues without CSP or change of intensity are shown in grey, residues with significant CSP are shown in red.

(D) Chemical shift perturbations of Hsp90 $^{13}\text{CH}_3$ -IM resonances upon addition of unlabeled NudC $^{1-274}$. Bar graphs showing CSPs of Hsp90 labeled residues along the sequence. Residues without CSP or change of intensity are shown in grey, residues with significant CSP are shown in red.

- (E)** Chemical shift perturbations of Hsp90 $^{13}\text{CH}_3$ -IM resonances upon addition of unlabeled NudC¹⁻¹⁴¹. Bar graphs showing CSPs of Hsp90 labeled residues along the sequence. Residues without CSP or change of intensity are shown in grey.
- (F)** Chemical shift perturbations of Hsp90^{MD} ^1H - ^{15}N resonances upon addition of unlabeled NudC¹⁵⁸⁻²⁷⁴. Bar graphs showing CSPs of Hsp90^{MD} residues along the sequence. Residues with significant CSP (>0.043) are shown in red, otherwise residues are shown in light green.
- (G)** Representation of significantly perturbed residues on Hsp90^{MD} structure. Surface representation of the structure of Hsp90^{MD} extracted from PDB: 5FWK. Residue color-coding follows the one used in panel F.
- (H)** Chemical shift perturbations of NudC¹⁵⁸⁻²⁷⁴ ^1H - ^{15}N resonances upon addition of unlabeled Hsp90^{MD}. Bar graphs showing CSPs of NudC¹⁵⁸⁻²⁷⁴ residues along the sequence. Residues with significant CSP (>0.072) are shown in blue, otherwise residues are shown in red.
- (I)**, Representation of significantly perturbed residues on NudC^{CS} structure. Surface representation of the structure of NudC¹⁵⁵⁻²⁷⁴ (PDB: 3QOR). Residue color-coding follows the one used in panel H.
- (J)** Overlaid chemical shift perturbations of Hsp90^{MD} ^1H - ^{15}N resonances upon addition of either unlabeled NudC¹⁵⁸⁻²⁷⁴ or NudC¹⁵⁸⁻³³¹. Bar graphs showing CSPs of Hsp90^{MD} along the sequence. Light green bar graph shows CSPs upon addition of NudC¹⁵⁸⁻²⁷⁴ and purple bar graph shows CSPs upon addition of NudC¹⁵⁸⁻³³¹.
- (K)** Overlaid chemical shift perturbations of either NudC¹⁵⁸⁻²⁷⁴ or NudC¹⁵⁸⁻³³¹ ^1H - ^{15}N resonances upon addition of Hsp90^{MD}. Bar graphs showing CSPs of NudC along the sequence. Light orange bar graph shows CSPs on NudC¹⁵⁸⁻²⁷⁴ upon addition of Hsp90^{MD} and purple bar graph shows CSPs on NudC¹⁵⁵⁻³³¹ upon addition of Hsp90^{MD}.
- (L)** The binding of NudC to Hsp90 β ^{322-328GS}. The interaction of labeled NudC* to Hsp90 β and the Hsp90 β ^{322-328GS} mutant was analyzed by aUC in the absence of nucleotides. [NudC*: 500 nM].

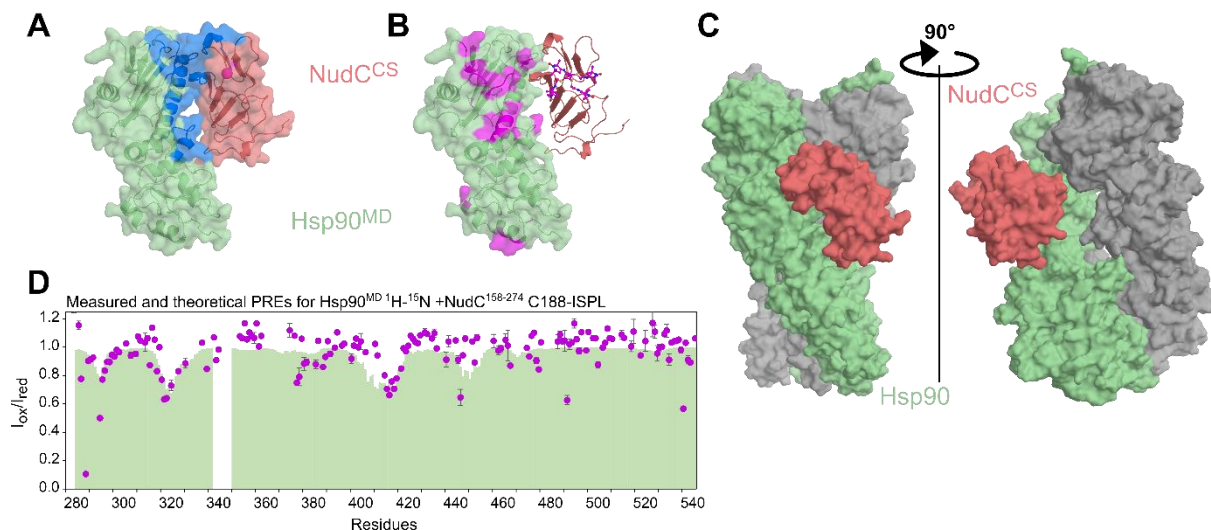


Figure S5: HADDOCK model of the Hsp90-MD NudC-CS complex (Related to Figure2)

(A) Representative structure of the best scored cluster obtained from HADDOCK modeling of the Hsp90^{MD} complex with NudC^{CS}. Active and passive residues used for the docking and selected based on CSPs and solvent accessibility are shown in blue on the surface of Hsp90^{MD} (light green) and of the NudC^{CS} domain (red).

(B) Representative structure of the best model cluster obtained from HADDOCK modeling of the Hsp90^{MD} and NudC^{CS} complex. Significant PREs (<0.82) are colored magenta on the surface rendering of the Hsp90^{MD}. The IPSL spin-label is shown as sticks on the NudC^{CS}.

(C) Superposition of the Hsp90^{MD} / NudC^{CS} complex with the structure of the closed conformation Hsp90 (PDB: 5FWK (Verba et al., 2016)) showing that the CS domain of NudC only interacts with one of the two protomers.

(D) Experimentally measured vs. back-calculated PREs observed for amide signals in ¹⁵N labeled Hsp90^{MD} bound to NudC^{CS} IPSL-labeled at C188. Experimental PREs are shown as magenta dots, with errors calculated based on the signal/noise ratio in the NMR spectra. The green surface shows the average PREs calculated for the four structures selected by HADDOCK with an ensemble of four conformations of the IPSL tag.

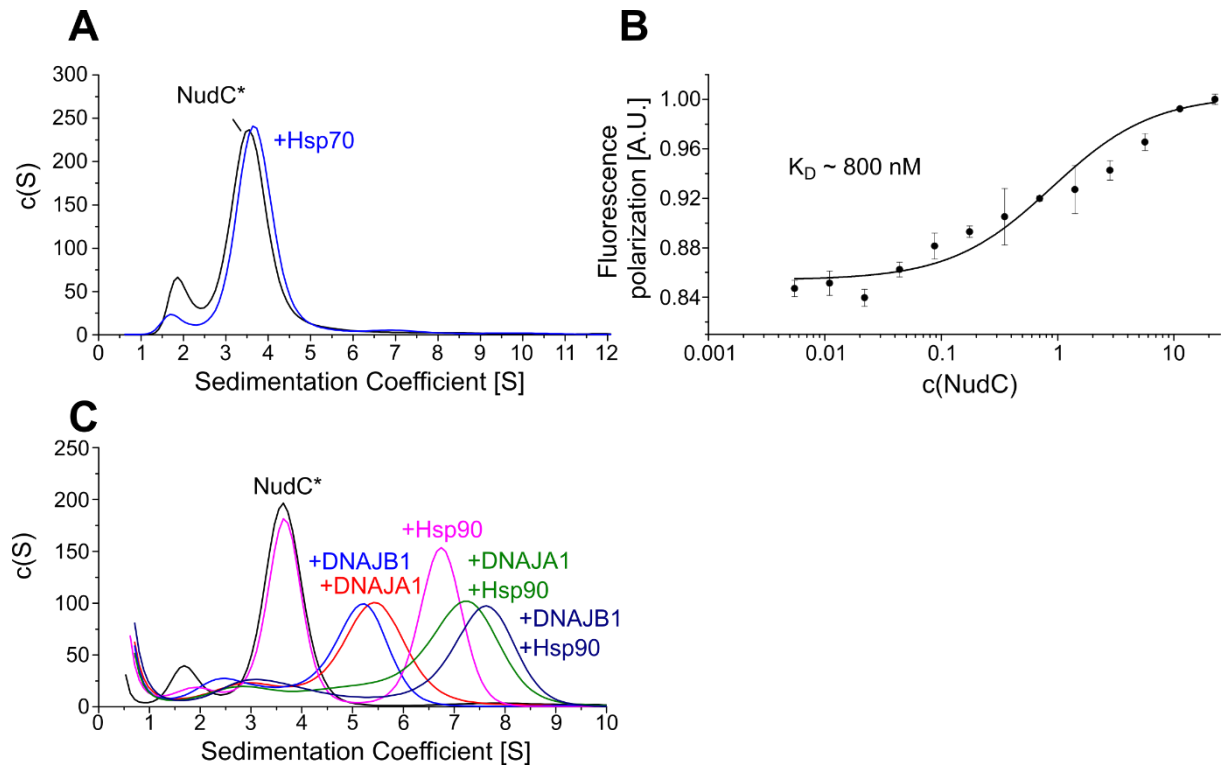


Figure S6: NudC binds Hsp40 *in vitro* (Related to Figure 3)

(A) NudC does not bind Hsp70. The binding of labeled NudC* to Hsp70 was analyzed by aUC. Binding was analyzed in the presence of 2 mM ATP. [NudC*: 500 nM, Hsp70: 3 μM].

(B) NudC binds Hsp40 with high affinity. The interaction between labeled yeast Hsp40 (Ydj1) and NudC was analyzed by fluorescence polarization. The binding was analyzed using a one single-site binding model. Shown are the means \pm SD of two replicates.

(C) NudC also binds human Hsp40. The sedimentation coefficient distribution of an aUC experiment with labelled NudC* and human DNAJA1 and DNAJB1 is shown. The experiment was conducted in the absence of nucleotides. [NudC*: 500 nM, DNAJA1: 4 μM , DNAJB1: 4 μM , Hsp90 α : 4 μM].

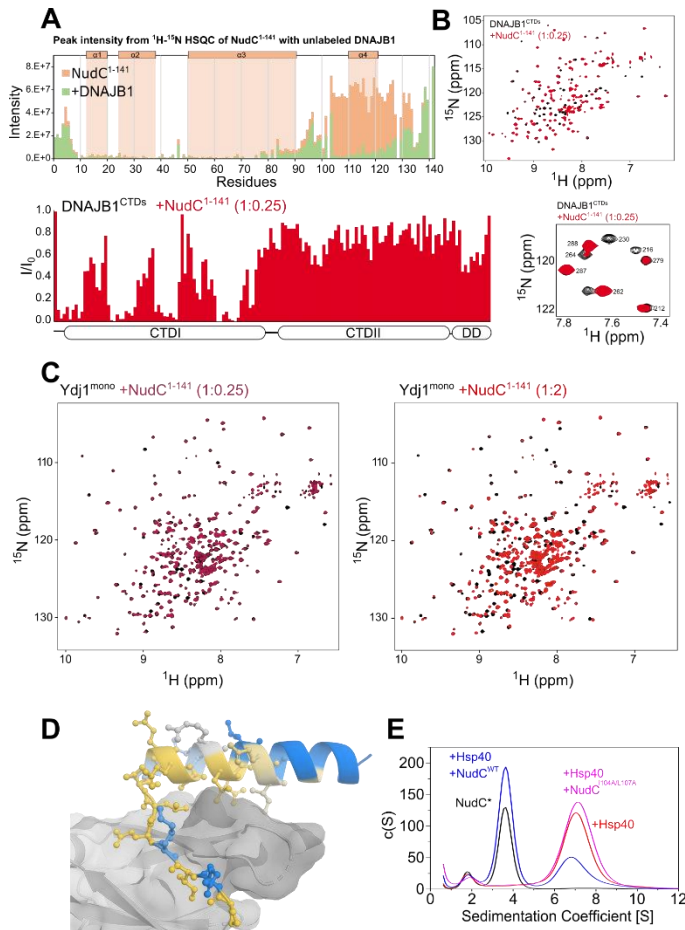


Figure S7: Interaction of NudC with Hsp40 (Related to Figure 3)

(A) Raw intensities of ^1H - ^{15}N resonances of NudC $^{1-141}$ upon addition of DNAJB1. The locations of the helices $\alpha 1$ to $\alpha 4$ are indicated.

(B) (Top) ^1H - ^{15}N HSQC spectrum of 0.2 mM DNAJB1 alone (black), and with 0.05 mM ^1H NudC $^{1-141}$ (red). Selective peak broadening can be seen, indicating binding. (Bottom right) Selected region of the HSQC spectra, with assigned peaks showing selective binding. (Bottom left) Residue-resolved NMR signal intensity ratio I/I_0 , where I and I_0 are signal intensities for DNAJB1 bound to NudC $^{1-141}$, and alone.

(C) (Left) ^1H - ^{15}N HSQC spectra of 0.2 mM Ydj1 alone (black), and with 0.05 mM ^1H NudC $^{1-141}$ (dark red). Selective peak broadening can be seen, indicating binding. (Right) ^1H - ^{15}N HSQC spectra of 0.2 mM Ydj1 CTDs mono alone (black), and with 0.4 mM ^1H NudC $^{1-141}$ (red). At higher concentrations of NudC new resonances appear, suggesting that the interaction happens at an intermediate exchange time scale.

(D) Conservation of NudC residues involved in Hsp40 binding. The degree of conservation of NudC residues involved in the binding of Hsp40 were determined using ConSurf and plotted on the crystal structure. Yellow color shows strong conservation and blue color indicates less conserved residues.

(E) Role of NudC I104 and L107 in Hsp40 binding. Atto488-labeled NudC* was bound to yeast Hsp40 in the presence of excess unlabeled NudC $^{\text{WT}}$ or NudC $^{\text{I104A/L107A}}$ and analyzed by analytical ultracentrifugation. The experiment was conducted in the absence of nucleotides. [NudC*: 500 nM, Hsp40 (Ydj1): 3 μM , NudC and NudC mutant: 10 μM].

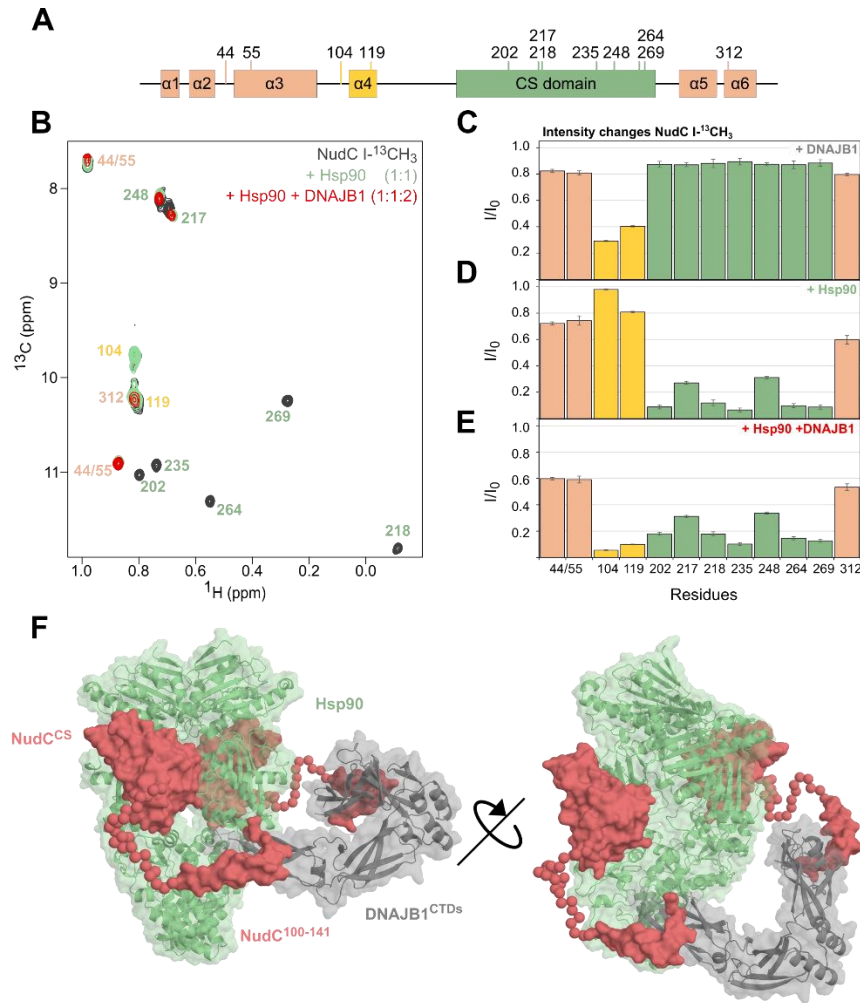


Figure S8: NudC links Hsp40 to Hsp90 (Related to Figure 4)

(A) Topology of NudC with the position of isoleucines indicated. The N-terminal and C-terminal helices are indicated light orange, the helix $\alpha 4$ is shown in yellow and the CS domain is indicated in light greens.

(B) NudC Ile- $^{13}\text{CH}_3$ methyl-TROSY spectrum. Overlay of the ^1H - ^{13}C HMQC spectrum of NudC alone (black), after addition of unlabeled Hsp90 (green) and after addition of unlabeled Hsp90 and DNAJB1 (red). Peak labels are colored based on NudC topology.

(C) Bar graph showing peak intensity changes of NudC I- $^{13}\text{CH}_3$ upon addition of DNAJB1 along its sequence. The bars are colored according to NudC topology. Error is calculated based on the signal/noise ratio of the spectra.

(D) Bar graph showing peak intensity changes of NudC I- $^{13}\text{CH}_3$ upon addition of Hsp90 along its sequence. The bars are colored according to NudC topology.

(E) Bar graph showing peak intensity changes of NudC I- $^{13}\text{CH}_3$ upon addition of Hsp90+DNAJB1 along its sequence. The bars are colored according to NudC topology.

(F) Model based on the HADDOCK model of the Hsp90^{MD}/ NudC^{CS} complex and the NudC¹⁰⁰⁻¹⁴¹/DNAJB1^{CTDs} crystal structure in which dummy residues generated in a random coil represent the sequence 142-154 connecting the helix $\alpha 4$ to the CS domain of NudC. The model represents a possible 2:2:2 interaction between the three proteins, consistent with our NMR data. Note that this model lacks the NudC dimerization domain and the Hsp40 J-domain, since they are not present in the underlying structures used for the model.

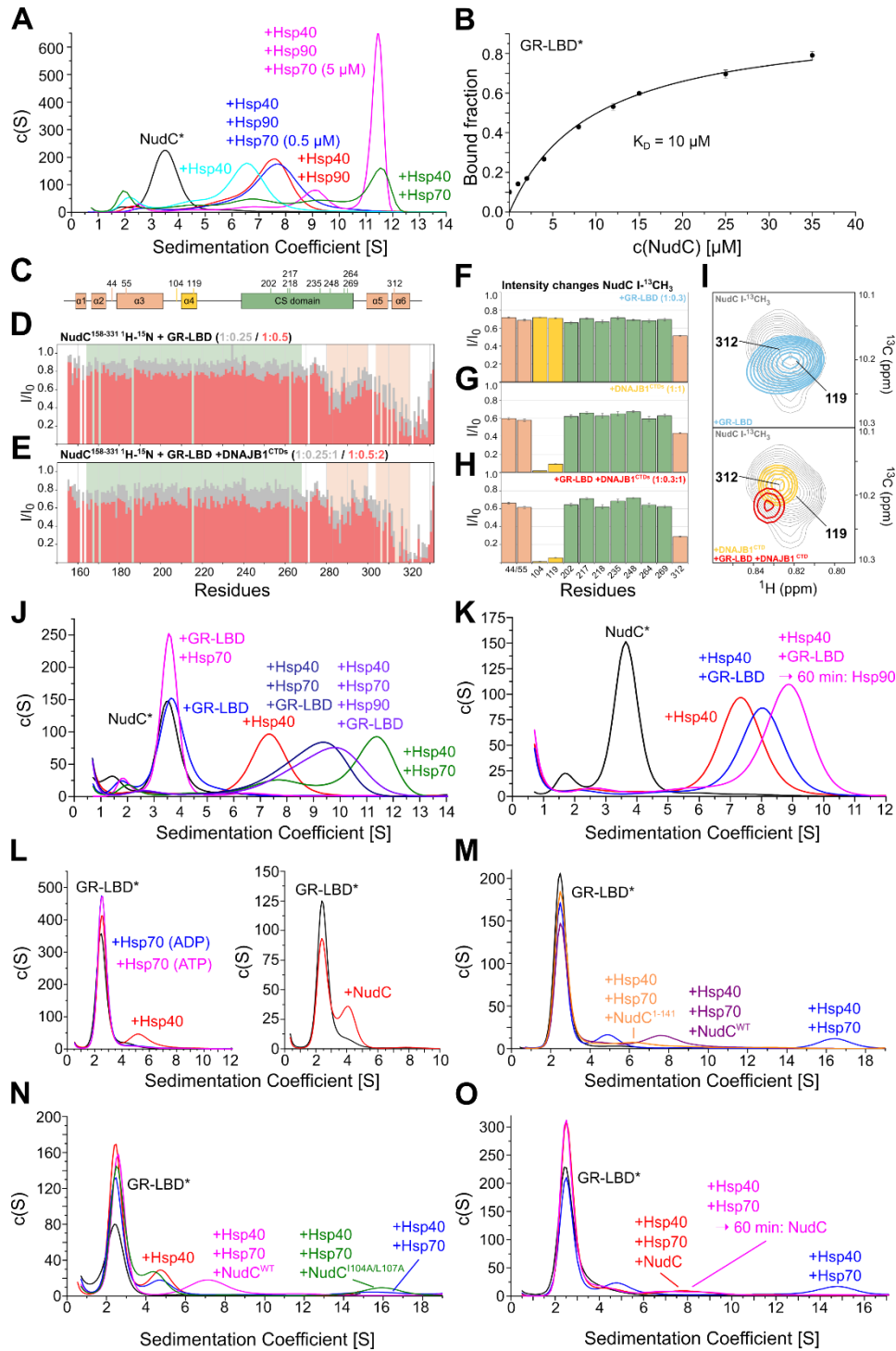


Figure S9: The interaction of NudC with the client transfer complex between Hsp40/Hsp70 and Hsp90 (Related to Figure 4)

(A) NudC does not bridge Hsp40/Hsp70 and Hsp90. The sedimentation coefficient distribution of aUC experiments with labelled NudC* and the indicated components is shown. Different Hsp70 concentrations were used as indicated. The experiments were performed in the presence of 2 mM ATP. [NudC*: 500 nM, Hsp40 (Ydj1): 4 μM, Hsp90α: 4 μM, Hsp70: 3 μM or as indicated].

(B) NudC directly binds GR-LBD with low affinity. Unlabeled NudC was titrated to labelled GR-LBD* and the bound fraction was quantified by aUC. Shown are the means \pm SD of three independent titrations. [GR-LBD*: 500 nM].

(C) Topology of NudC with the position of isoleucines indicated.

(D) Intensity changes in ^1H - ^{15}N resonances of NudC¹⁵⁸⁻³³¹ upon addition of GR-LBD. Topology is indicated at the top of the graph. Two different concentration points were performed, a NudC/GR molar ratio of 1:0.25 (grey) or 1:0.5 (red).

(E) Intensity changes in ^1H - ^{15}N resonances of NudC¹⁵⁸⁻³³¹ upon addition of premixed GR-LBD with a large excess of DNAJB1^{CTDs}. Topology is indicated at the top of the graph. Two different concentration points were performed, a NudC/GR/DNAJB1 molar ratio of 1:0.25:2 (grey) or 1:0.5 (red).

(F) Bar graph showing peak intensity changes of NudC I- $^{13}\text{CH}_3$ upon addition of GR-LBD along its sequence.

(G) Bar graph showing peak intensity changes of NudC I- $^{13}\text{CH}_3$ upon addition of DNAJB1^{CTDs} along its sequence.

(H) Bar graph showing peak intensity changes of NudC I- $^{13}\text{CH}_3$ upon addition of premixed GR-LBD and DNAJB1^{CTDs} along its sequence.

(I) Extract of NudC Ile- $^{13}\text{CH}_3$ methyl-TROSY spectrum. Overlay of the ^1H - ^{13}C HMQC spectrum of NudC alone (black), after the individual addition of unlabeled GR-LBD (blue), DNAJB1^{CTDs} (yellow) or of these two proteins simultaneously (red). The resonance of I312 shows a specific shift upon interaction with GR-LBD, that is conserved when DNAJB1^{CTDs} is added simultaneously.

(J) The interaction of NudC with different components. Controls for the binding of labeled NudC* to the shown components were analyzed by aUC in the presence of 2 mM ATP. [NudC*: 500 nM, Hsp40 (Ydj1): 4 μM , GR-LBD: 4 μM , Hsp70: 3 μM , Hsp90 α : 4 μM].

(K) NudC can recruits GR-LBD:Hsp40 complexes to Hsp90. NudC*, Hsp40 and GR-LBD were mixed and incubated for 60 min at room temperature to form NudC*:Hsp40:GR-LBD complexes before Hsp90 was added and the sample was analyzed by aUC. [NudC*: 500 nM, Hsp40 (Ydj1): 4 μM , GR-LBD: 4 μM , Hsp90 α : 5 μM]. **I**, The GR-LBD does not directly bind Hsp70. (Left panel) The binding of labeled GR-LBD* to Hsp70 is shown in the presence of 2 mM ADP or ATP as determined by aUC. The binding to Hsp40 is shown as a control. (Right panel) The binding of GR-LBD* to 6 μM NudC is shown. [GR-LBD*: 500 nM, Hsp40 (Ydj1): 4 μM , Hsp70: 3.5 μM , NudC: 6 μM].

(M) NudC leads to the disruption of the Hsp40:Hsp70:client complex. The sedimentation curves of labelled GR-LBD* with the indicated components in an aUC experiment are shown. The experiments were conducted in the presence of 2 mM ATP. [GR-LBD*: 500 nM, Hsp40 (Ydj1): 4 μM , Hsp70: 3 μM , NudC and mutant: 5 μM].

(N) The disruption of Hsp40:Hsp70:client complexes requires the interaction of NudC with Hsp40. The aUC sedimentation curves of labelled GR-LBD* with the indicated components are shown. The experiments were conducted in the presence of 2 mM ATP. [GR-LBD*: 500 nM, Hsp40 (Ydj1): 4 μM , Hsp70: 3 μM , NudC and mutant: 6 μM]. **o**, NudC disrupts pre-formed GR-LBD:Hsp40:Hsp70 complexes. GR-LBD*, Hsp40 and Hsp70 were incubated for 60 min at room temperature in the presence of ATP to form GR-LBD*:Hsp40:Hsp70 complexes. NudC was then added and the sample was analyzed by aUC. [GR-LBD*: 500 nM, Hsp40 (Ydj1): 4 μM , Hsp70: 3 μM , NudC: 5 μM].

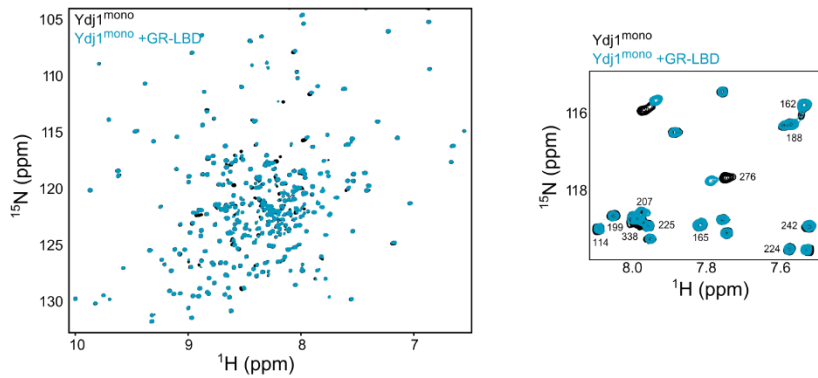
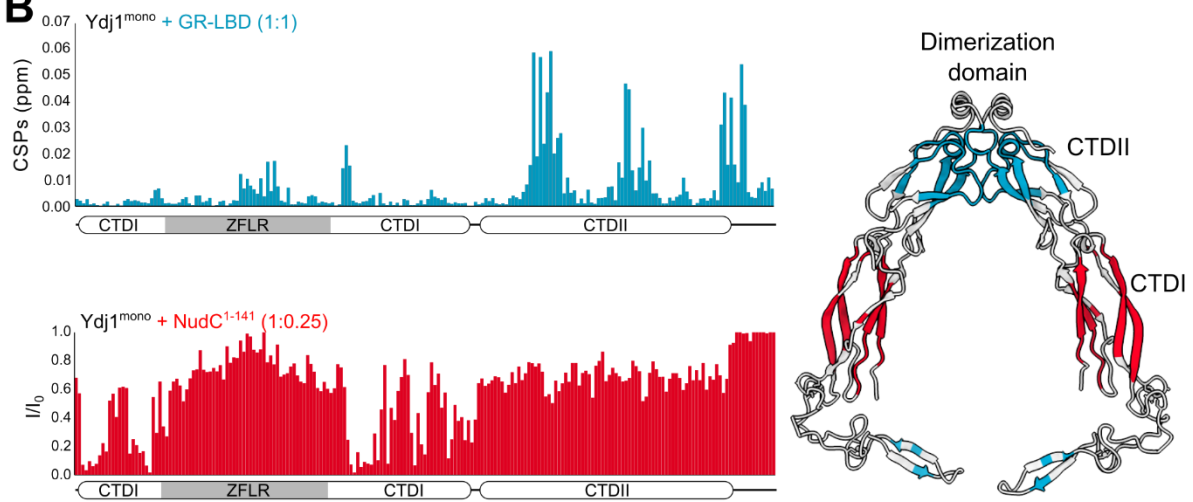
A**B**

Figure S10: The interaction of the GR-LBD with yeast Hsp40 (Ydj1) (Related to Figure 4)

(A) (Left) ^1H - ^{15}N HSQC spectra of 0.12 mM Ydj1 alone (black), and with 0.12 mM ^1H GR-LBD (blue). Chemical shift perturbations can be seen, indicating selective binding. (Right) Selected region of the HSQC spectra in A, with assigned peaks showing selective binding.

(B) (Top) Residue-resolved NMR chemical shift perturbations (CSPs) of Ydj1 bound to GR-LBD. Binding regions are areas with a significant shift and are localized to CTDII. (Bottom) Residue-resolved NMR intensity ratios of Ydj1 bound to NudC¹⁻¹⁴¹ showing binding to CTDI. CSPs and I/I_0 signals from the residue-resolved bar graphs have been plotted on the structure of Ydj1 (PDB: 1NLT).

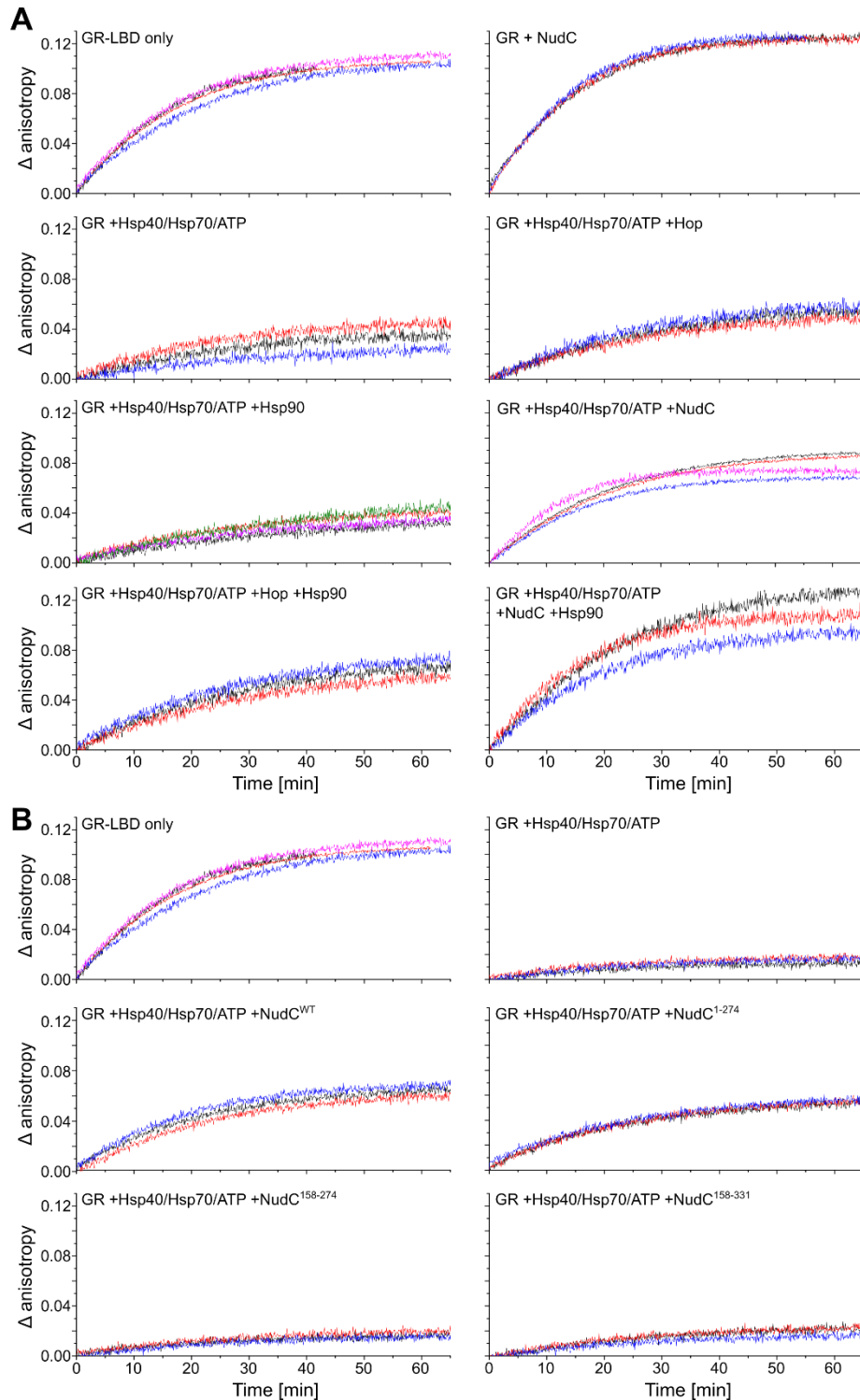


Figure S11: NudC promotes the binding of hormone to GR-LBD (Related to Figure 5)

(A) Individual fluorescence anisotropy traces measuring hormone binding to the GR-LBD. The apo GR-LBD (GR) was mixed with the indicated (co-)chaperones and incubated for 60 min before adding F-Dex and monitoring fluorescence anisotropy. The data refer to the bar chart in Figure 5C.

(B) Individual fluorescence anisotropy traces measuring hormone binding to the GR-LBD. The apo GR-LBD (GR) was mixed with the indicated (co-)chaperones and incubated for 60 min before adding F-Dex and monitoring fluorescence anisotropy. Note that the GR only control traces from **A** were used as a reference. The data refer to the bar chart in Figure 5D.

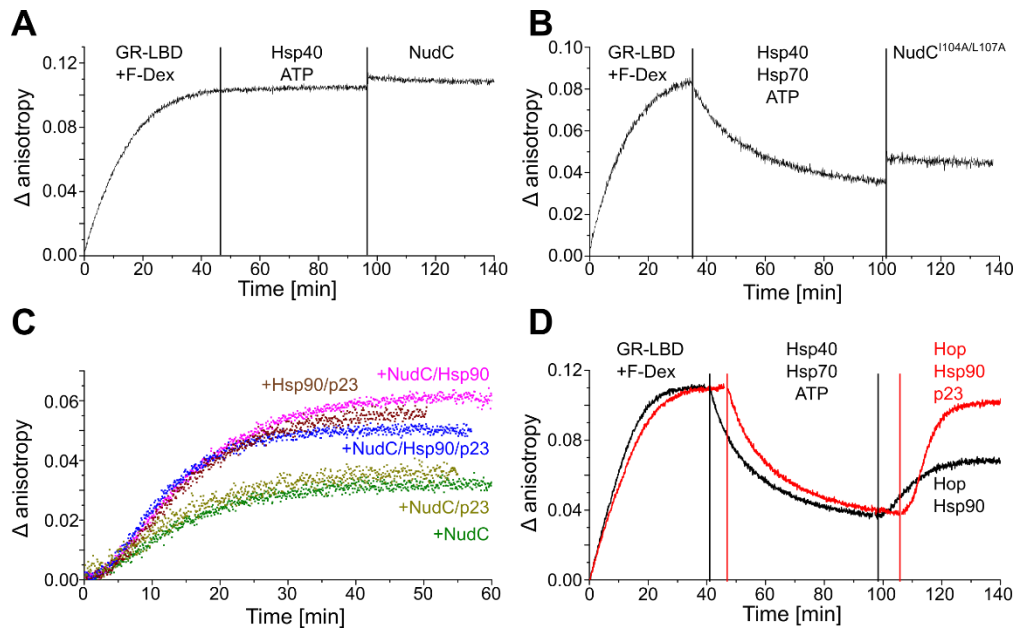


Figure S12: Hormone binding recovery by NudC depends on Hsp70 release from the GR-LBD (Related to Figure5)

(A) Hsp70 is required to dissociate hormone from the GR-LBD. The fluorescence anisotropy of 100 nM F-Dex was monitored as a function of time as different components were added. Initially, F-Dex binding was observed in the presence of 1 μ M apo GR-LBD. After 46 minutes, Hsp40 (1.83 μ M) and 4.6 mM ATP were added. No dissociation of hormone was observed. After 97 minutes, NudC was added. Again, no change in the anisotropy of F-Dex was observed. Vertical lines indicate the time at which the indicated components were added.

(B) The interaction of NudC with Hsp40 is required to release Hsp70 from the GR-LBD. The fluorescence anisotropy of 100 nM F-Dex was monitored as a function of time as different components were added. Initially, F-Dex binding was observed in the presence of 1 μ M apo GR-LBD. After 35 minutes, Hsp40 (1.83 μ M), Hsp70 (11.1 μ M) and 4.6 mM ATP were added leading to the release of F-Dex. After 102 minutes, NudC^{I104A/L107A}, which cannot bind Hsp40, was added. No gain in the functionality of GR-LBD was observed. Vertical lines indicate the time at which the indicated components were added.

(C) p23 is not required in the NudC-mediated client maturation pathway. The kinetics of F-Dex (100 nM) binding to the apo GR-LBD (1 μ M) pre-incubated with Hsp40 (1 μ M), Hsp70 (12 μ M), ATP (5 mM) and the shown (co)-chaperones for 60 min at room temperature are shown. F-Dex binding to the GR-LBD was analyzed by fluorescence anisotropy. The initial fluorescence anisotropy value immediately after addition of F-Dex was set to 0.

(D) p23 is required for the Hop-mediated client maturation pathway. A timed-addition experiment measuring hormone binding to the GR-LBD is shown. Hormone binding was analyzed by the change of fluorescence anisotropy as a function of time. Apo GR-LBD (1 μ M) was first bound to F-Dex (100 nM) and after about 45 minutes hormone was released by Hsp40 (1.83 μ M), Hsp70 (11.1 μ M) and ATP (5 mM). Hormone rebinding was observed after the addition of Hop (10 μ M), Hsp90 (12 μ M) and p23 (12 μ M) after about 100 minutes as indicated. The immediate y-offset caused by addition of Hsp90, Hop and p23 was corrected. Vertical lines indicate the time at which components were added and are color-coded as the traces.

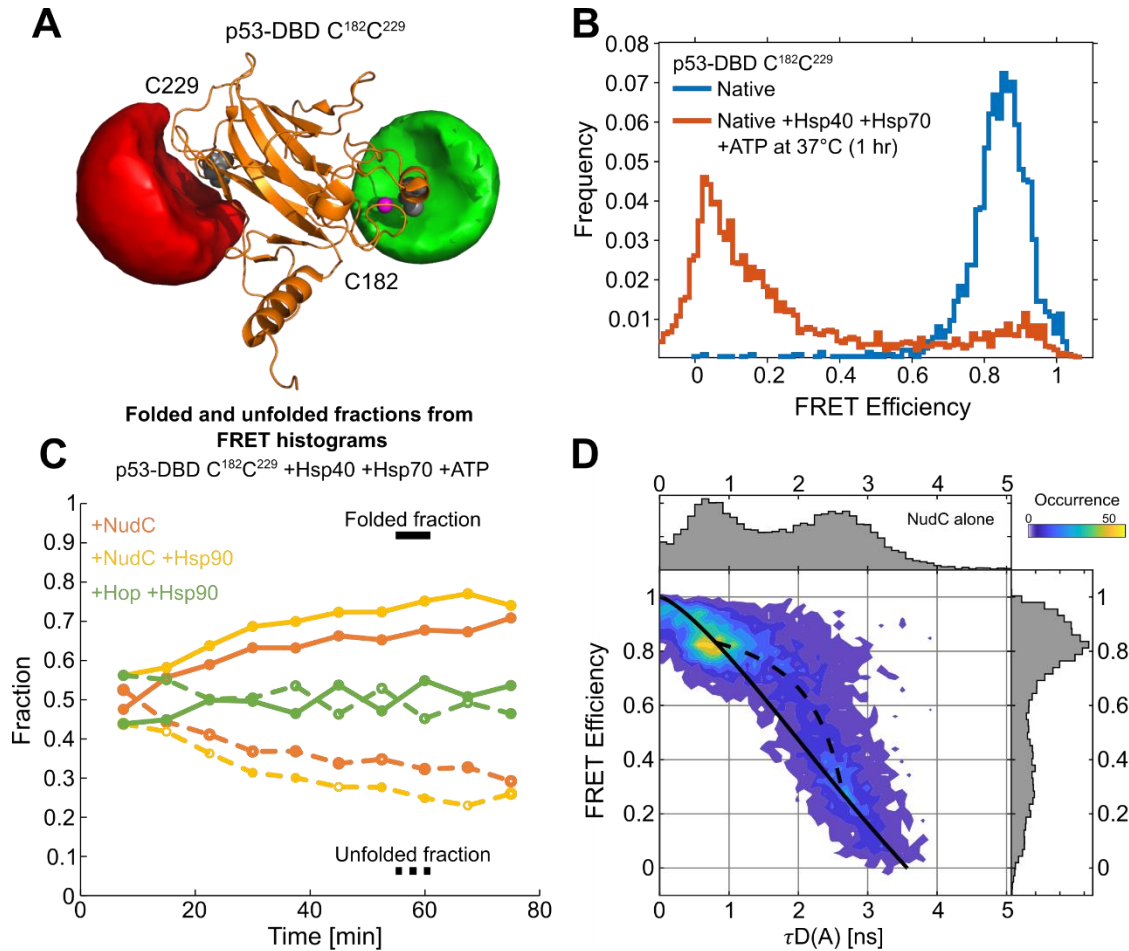


Figure S13: NudC promotes the folding of the p53-DBD (Related to Figure 5)

(A) p53-DBD FRET system. Accessible volume calculations for the used dyes Atto532 (green) and Alexa647 (red) at the labelling positions C182 and C229 (shown in the dark spheres) on the p53-DBD structure (PDB: 1UOL) (Dahiya et al., 2019). Dyes were labeled stochastically. The zinc ion is displayed in magenta.

(B) The p53-DBD is unfolded by the Hsp40/Hsp70 system. The spFRET histograms of native p53-DBD^{C182/C229} (blue) and p53-DBD^{C182/C229} in the presence of Hsp40/Hsp70 (red) are shown.

(C) NudC increases the population of folded p53-DBD. The kinetics of the folding reaction of p53-DBD^{C182/C229} in the presence of the indicated (co)-chaperones were measured from spFRET experiments binned with a time resolution of 7.5 min. Folding of Hsp40/Hsp70 bound p53-DBD^{C182/C229} was followed after the addition of NudC (orange), NudC and Hsp90 (yellow) and Hop and Hsp90 (green). We separated the folded and unfolded fractions of the proteins using a FRET efficiency value of 0.55. Proteins with a higher FRET efficiency were considered folded, those below were considered unfolded. Solid line connects the data points for folded fractions and dotted line for unfolded fractions.

(D) The presence of the dynamics in NudC mediated p53-DBD folding. A 2D histogram showing the FRET efficiency vs donor fluorescence lifetime in the presence of an acceptor is depicted for p53-DBD upon addition of 10 μ M NudC after pre-incubation with 2 μ M Hsp40 and 10 μ M Hsp70 for 1 hour. The solid black line indicates the ideal relationship between FRET efficiency and donor lifetime assuming a single, static FRET efficiency. Static molecules fall on this line, while molecules on the dashed line exhibit dynamics attributed to NudC induced release and rebinding of p53-DBD from Hsp40/Hsp70.

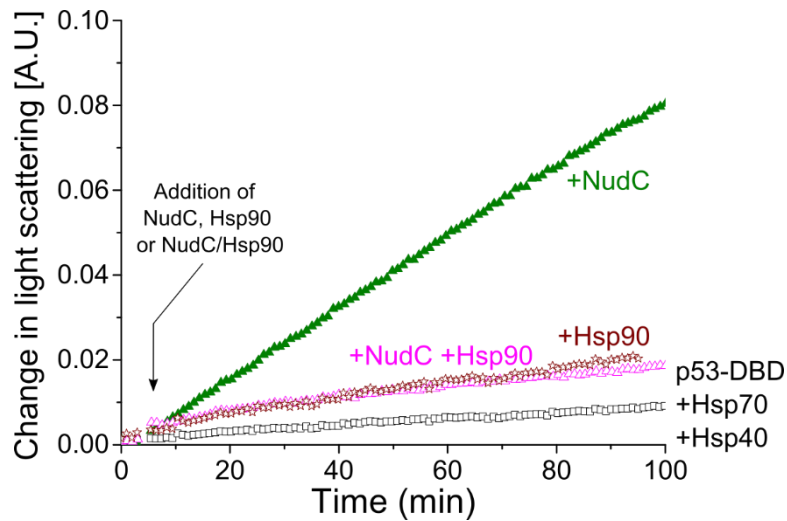


Figure S14: NudC cooperates with Hsp90 to suppress p53-DBD aggregation (Related to Figure 5)

Aggregation of p53-DBD in the presence of (co)-chaperones. p53-DBD was incubated with Hsp40, Hsp70 and ATP at 37 °C before addition of the indicated (co)-chaperones. Aggregation was analyzed by measuring the light scattering signal.

Supplementary Table 1: Sedimentation coefficients of complexes in aUC experiments (Related to Figure 4)

Components	Sedimentation Coefficient
NudC*	~ 3.6 S
NudC* +Hsp40 (Ydj1)	~ 7 S
NudC* +Hsp40 (Ydj1) +Hsp70	~ 11 S
NudC* +Hsp90 (apo)	~ 7 S
NudC* +Hsp40 (Ydj1) +GR-LBD	~ 7.5 S
NudC* +Hsp40 (Ydj1) +Hsp90	~ 7.7 S
NudC* +Hsp40 (Ydj1) +Hsp90 +GR-LBD	~ 8 S
GR-LBD*	~ 2.5 S
GR-LBD* +Hsp40 (Ydj1)	~ 5 S
GR-LBD* +NudC	~ 4.2 S
GR-LBD* +Hsp90 (apo)	~ 7 S
GR-LBD* +Hsp40 (Ydj1) +Hsp70	~ 16.5 S
GR-LBD* +Hsp40 (Ydj1) +NudC	~ 7.5 S
GR-LBD* +Hsp40 (Ydj1) +NudC ¹⁻¹⁴¹	~ 6 S
GR-LBD* +Hsp40 (Ydj1) +NudC +Hsp90	~ 8 S

Supplementary Table 2: Data collection and refinement statistics (Related to Figure 3)

DNAJB1 ^{CTDs} /NudC ¹⁰⁰⁻¹⁴¹	
Data collection	
Space group	I2 ₁ 2 ₁ 2 ₁
Cell dimensions	
<i>a</i> , <i>b</i> , <i>c</i> (Å)	41.30, 128.26, 135.21
α , β , γ (°)	90.00, 90.00, 90.00
Resolution (Å)	46.53-2.54 (2.65-2.54)
<i>R</i> _{merge}	0.145 (1.862)
CC (1/2)	0.999 (0.661)
<i>I</i> / σ <i>I</i>	16.5 (1.6)
Completeness (%)	99.9 (99.2)
Redundancy	13.0 (13.1)
Refinement	
Resolution (Å)	46.57-2.54
No. reflections	12295
<i>R</i> _{work} / <i>R</i> _{free}	0.23 / 0.27
No. atoms	
Protein	1430
Ligand/ion	16
Water	22
B-factors	
Protein	74.17
Ligand/ion	88.82
Water	51.19
R.m.s. deviations	
Bond lengths (Å)	0.015
Bond angles (°)	2.18

Supplementary Table 3 : CRISPRi screen protospacer sequences and results (Related to STAR Methods)